Spectroscopic and theoretical study of the pH effect on the optical properties of the calcium–morin system

Diksha Jani Thaviligadu, Luc Labarrière, Aurélien Moncomble, Jean-Paul Cornard

Spectroscopic and theoretical study of the pH effect on the optical properties of the calcium–morin system

Diksha Jani Thaviligadu, Luc Labarrière, Aurélien Moncomble, Jean-Paul Cornard*

Univ. Lille, CNRS, UMR 8516 - LASIR - Laboratoire de Spectrochimie Infrarouge et Raman, F-59000 Lille, France

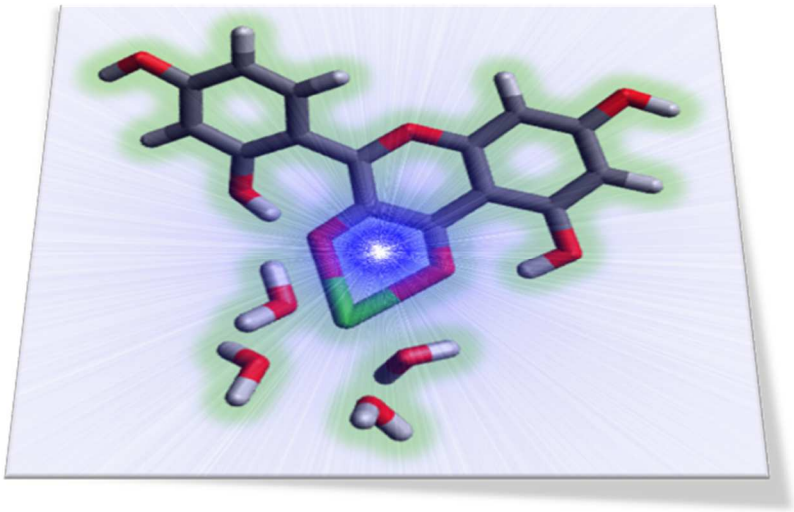

Abstract:

Morin (2-(2,4-dihydroxyphenyl)-3,5,7-trihydroxychromen-4-one) is an abundant flavonoid with various pharmacological and biological activities. Considering the ubiquitous presence of calcium cations in biological systems, it seems relevant to study the interaction of this ion with morin and the influence of pH on this system. In a first step, among the four hypothetical chelation sites, the preferential fixing site, its protonation state and the Ca environment have been determined by combining electronic spectroscopies and density functional theory (DFT) and time-dependent DFT calculations. Then, using the same methodology, the fate of the formed complex with the variation of pH was studied. Calcium chelation occurs with the 3-hydroxy-4-keto site with deprotonation of the hydroxyl group. The coordination number of Ca^{II} does not seem to be a determining parameter insofar whatever the number of solvent molecules present in the coordination sphere of the metal, the calculation of the electronic transitions leads to the same results. With the increase in pH, a first deprotonation of the complex occurs at the level of a solvent molecule in the metal coordination sphere, followed by a deprotonation of the hydroxyl function in position 7.

*Corresponding author: jean-paul.cornard@univ-lille.fr

1. INTRODUCTION

For years now, a large number of complexation reactions have been studied to see the behavior of ligands in the presence of metal cations and to investigate the evolution of their physical properties.

Morin (2', 3, 4', 5, 7-pentahydroxyflavone) is a yellow pigment which forms part of the family of flavonoids.[1] These molecules are intensely studied as they are natural products that present excellent antioxidant[2-3], anti-inflammatory[4-5], antifungal[6] and neuroprotective[7] characteristics. Morin belongs to the polyphenol family and is found in fruits, vegetables, cereals and other substances like coffee seeds. Nowadays, different ways are being approached to enhance these features, one of them being the synthesis of their complexed form with certain metal cations.

Other than the fact that morin is a secondary metabolite, it is also a multisite ligand with several fixation sites available for the metal cations to position themselves. One of the most interesting features of morin is that it contains one chelating site which is seldom present in the compounds of the family and which moreover is rarely taken into consideration in the literature. Fig. 1 represents the structure, the atomic numbering and the chelating sites of morin. While the α-hydroxyketo (positions 3 and 4), β-hydroxyketo (positions 4 and 5) and hydroxyether (positions 1 and 2') sites are already established, another site can be obtained when the bond connecting the rings B and C is rotated. This diol site is situated between the positions 3 and 2'. On the top of that, this conformer is favored since a network of intramolecular hydrogen bonds is created between the positions 2', 3 and 4.[8]

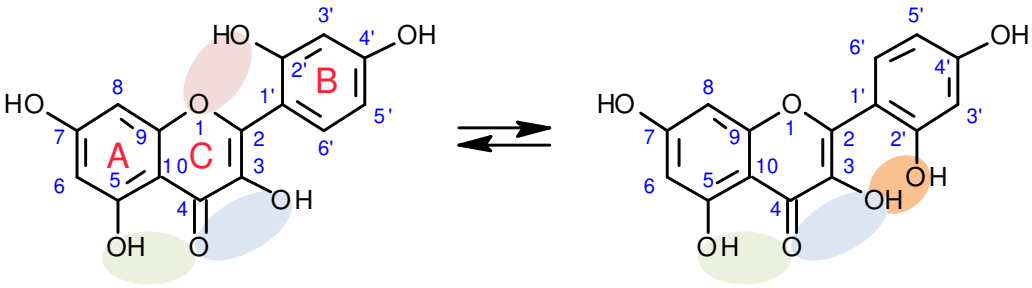

Figure 1: Chemical structure, atomic numbering, ring nomenclature and potential metal chelating sites of morin.

The complexation of different metal cations by morin has been the subject of various studies.[9-15] However, in no case the diol function was considered. The metal chelation is likely to significantly alter the biological properties of the flavonoid.[16-19]

In general, transition metals are the elements of interest for these types of reactions. They possess d orbitals that facilitate the formation of coordination complexes. However, in this study, emphasis was put on the calcium cation, which is rarely used despite the fact that it is widely present in soil and is essential in the human body.

Being one of the most abundant elements present in the Earth crust, it is available in many areas worldwide mostly in the form of salts. These ions are useful for the environment as they represent one of the required constituent for the growth of plants. The calcium ions present in the soil is taken up by the xylem.[20] The amount of the mineral taken depends on the cation exchange capacity of the root cell walls and this movement is regulated to prevent an excess of Ca^{II} in the shoots that can easily hinder the growth of plants. On another note, a deficiency in the cationic mineral generally occurs in tomatoes, green leaves like lettuces, celery and especially in plants that are fed by the phloem instead of the xylem. Ca^{2+} plays an essential role in maintaining the integrity of cell walls and cell membranes. As a positively-charged ion, not only does it act as a counter cation with respect to the anions in the vacuoles of the cells but it also combines with proteins to allow the transduction of the cytosolic Ca^{II} concentration signal.[21]

Calcium is also known to be the most abundant metal in an individual, constituting 2% of the body weight. Calcium is one of the key factors not only in the regeneration of bones in our body but also in nerves and muscles function. Like other chemicals, a deficiency or an excess of Ca^{2+} can cause serious problems in the organism.[22-23] Ca^{2+} is essential for the human cell activities, acting as a secondary messenger to transmit biological information from one cell to the other.[24-25] As a matter of fact, the biochemical mechanism of the whole nervous system assimilates the concentration Ca^{2+} in its complex pathways. The cellular Ca^{2+} signaling occurs in the mitochondria. The intracellular concentration of Ca^{2+} is controlled by the mitochondria and also by specific Ca^{2+} binding proteins. This concentration is highly dependent on the proton electrochemical gradient, where the equilibrium is never attained due to the exchange occurring between H^+/Ca^{2+} and Na^+/Ca^{2+}. An improper regulation of the concentration can lead to mitochondrial dysfunction, defective production of ATP and even a rapid decrease in the lifespan of cells. Researches performed on animals showed that there is a direct relationship between the changes in Ca^{2+} concentration and mitochondrial misbalance, leading eventually to the Parkinson disease. In fact, one of the early features of the Parkinson disease could be due to the alteration of the Ca^{2+} homeostasis rather than neuronal malfunction.

The main objective of this paper is to study experimentally and theoretically the interaction of calcium cations with morin in order to investigate the type of complex formed. More specifically, the goal is to determine the morin site preferentially involved in calcium fixation and to study the influence of pH on the structure of the complex(es) formed. The experimental part of the work is done by electronic spectroscopy (both absorption and fluorescence emission spectroscopies). These techniques are appropriate to work with low concentrated solutions but not precise enough and they suffer from a lack of spectral information to provide structural information. To compensate for these shortcomings, quantum calculations are

performed and hence, a large amount of information is acquired for the system under study. This methodology has already been used with success on chemical systems of the same nature.[26-27]

2. Material and methods

2.1 Reagents and synthesis of metal complexes

Morin hydrate and calcium chloride hydrate were purchased from Sigma Aldrich. The experimental work was performed in methanol (ultrapure, spectrophotometric grade, 99.8%) purchased from Alfa Aesar. Water was obtained by a Millipore water purification system at 18 MΩ cm^{-1} for NaOH and HCl solutions. The method was optimized by preparing solutions of morin at a concentration of 4.10^{-5} mol L^{-1} and the calcium chloride solution was at 1.10^{-2} mol L^{-1}. The concentration of calcium chloride was chosen to obtain a broad range of molar ratios *R* (metal to ligand) varying from 0 to 50. The experiments related to morin were carried out at a fixed pH (4.2 and 6.2). 1 mol L^{-1}, 0.1 mol L^{-1} and 0.01 mol L^{-1} aqueous solutions of NaOH (white pellets, Fischer Scientific) and HCl (Fluka) were used to fix the pH during the titration. The stoichiometry of the formed complexes was determined by the molar ratio method and the spectral variations with the pH were studied at *R* constant.

2.2 Instrumentation and data treatment

All the experimental work was performed using electronic spectroscopy. A Varian Cary 300 Bio double beam spectrometer was used to record the absorption spectra and a Jobin Yvon Horiba Fluorolog spectrofluorometer was used to record the emission spectra. A Hanna pHmeter was used for pH measurements.

A set of titration measurements were carried out, with the addition of the calcium chloride solution in the reactor receptacle at different molar ratios of metal to ligand. The set-up was thereupon coupled, by means of a flow cell, to the spectrometers to follow the formation of the complex(es).

The set of spectra obtained was then treated using ReactLab Equilibria[28], a chemometrics tool designed to operate Evolving Factor Analysis (EFA).[29-30] From the data treatment, the spectra of morin and the formed complex were obtained and the apparent formation constants (β) were estimated. This constant results from the equilibrium between the free ligand L and the complex M_xL_y (without taking into account the protonation state of the ligand):

$$xM + yL = M_xL_y \qquad \beta = [M_xL_y]/([M]^x \cdot [L]^y)$$

2.3 Computational details

All the theoretical work was done using the Gaussian16 software[31], more precisely using the Density Functional Theory (DFT).[32] The structures of morin and the various plausible morin-Ca(II) complexes were optimized at the ground state using the B3LYP global hybrid functional[33-34] and the 6-311+G** basis set.[35-37] In total, 30 different structures of complexes were initially considered when varying the different fixation sites and its protonation state. Additional calculations were performed on some complexes to assess the effect of deprotonation of other groups not involved in the metal chelation, to simulate an increase in pH.

To represent the environment of the reaction, the Polarizable Continuum Model (PCM) model was implicitly associated to the system, with methanol as the solvent.[38-39]. Explicit water molecules were added around the calcium ion completing its coordination sphere. Indeed, we have shown that the presence of water molecules instead of methanol molecules has no effect on the calculations of electronic spectra.[40] To account for the influence of the coordination sphere on each complex, trials with 4, 3 and 2 molecules of water were performed.

Time Dependent Density Functional Theory (TD-DFT) was used to generate the electronic transitions in the range 200 nm to 600 nm. This will enable the overlap of the experimental absorbance spectra on the theoretical transitions for a good comparison. TD-DFT was also used to optimize the structure of excited states and to compute emission wavelengths. For absorption computation, the implicit solvent was equilibrated in the ground state while it was equilibrated in the excited state for emission.

3. Results

3.1. Complexation Reaction

The morin ligand in methanol solution presents the two main characteristic bands observed for all the flavonoids: band I located in the long wavelengths range at 357 nm and band II at 253 nm. These values are close to those reported in the literature.[41]

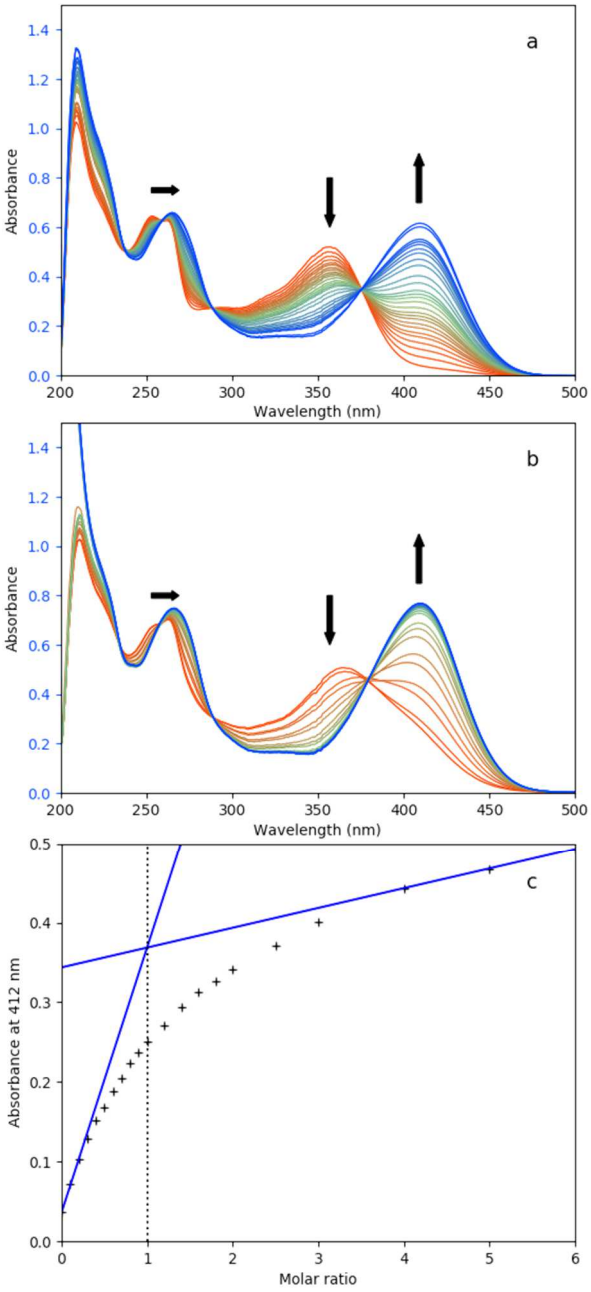

Figure 2: (a) Set of the UV-vis spectra of morin upon addition of Ca^{II} at pH = 4.2 for molar ratio varying from 0 to 20; (b) Set of the UV-vis spectra of morin upon addition of Ca^{II} at pH = 6.2 for molar ratio varying from 0 to 4 and (c) Absorbance versus molar ratio plots at 412 nm (pH = 6.2)

The spectral modifications observed on the UV-vis spectrum of morin upon addition of the calcium salt, at pH = 4.2, for molar ratio (metal/ligand) varying from 0 to 30 are illustrated in Fig. 2a. To ensure that the chemical equilibrium is reached, the spectrum was recorded 10 minutes after each metal addition. Bathochromic effects for both absorption bands are

observed with different amplitudes, showing the formation of the complex. While a shift of 53 nm is observed for band I (410 nm), a small shift of 11 nm is noticed for band II (264 nm). A weak absorption band is also detected at a wavelength of about 330 nm which will be noted band I'. The observation of several isobestic points (238, 259, 289 and 375 nm) in the spectra set indicates the presence of an equilibrium between two species in solution: the free ligand and a single complex. The same titration was carried out by fixing the pH value at 6.2 and the results are shown in Fig. 2b. The initial spectrum of the free ligand is different from the previous manipulation as it corresponds to the absorption of the totally protonated and mono-deprotonated forms simultaneously present in solution. However, the only formed complex (confirmed by the presence of isobestic points) has an absorption spectrum identical to the one obtained at a pH of 4.2. This result suggests that the same complex is formed for both pH values. For both titrations, the decrease in pH (readjusted after each addition of metal salt) means that Ca^{II} binding is accompanied by a deprotonation at the level of the complexation site. Our previous works have shown that the first deprotonation of morin occurs with the loss of the proton of the O2'H or O3H hydroxyl groups and the existence of an intramolecular hydrogen bond between these two functions in the conjugated base.[8] Irrespective of the protonation state of the free ligand (fully protonated or mono-deprotonated), the same spectral signature is obtained upon addition of Ca^{II}, showing that O2'H or O3H or both is involved in the metal binding. For instance, a chelation with the O4O5 site would lead to different complexes depending on the initial protonation state of morin. Therefore, the two possible chelation sites for Ca^{II} are the O3O4 fully deprotonated or O2'O3 mono-protonated or fully deprotonated. The molar ratio method applied for both pH at different wavelengths reveals the formation of a complex of stoichiometry 1:1 (To illustrate this example, the absorbance at 410 nm with respect to the $[Ca^{II}]/[morin]$ molar ratio for the titration performed at pH = 4.2 is reported in Fig. 2c). A model with a complex of stoichiometry 1:1 has been confirmed by chemometrics. The conditional stability constant for this complex at both pH values were estimated to be $\log \beta_{1:1} = 4.40 \pm 0.02$ and 6.87 ± 0.05 at pH = 4.2 and 6.2, respectively.

Fig. 3a illustrates the fluorescence EEM recorded for a Ca^{II}/morin solution for a molar ratio of 2 at pH = 4.2. Only one fluorescence peak can be observed in this matrix confirming the presence of a single complex in solution, morin not being fluorescent. The absence of dual fluorescence of the complex indicates that no excited state intramolecular proton transfer (ESIPT) occurs as it can be observed in 3-hydroxyflavone[42-44] or quercetin (3,5,7,2',3'-pentahydroxyflavone).[45-46] A possible explanation for the absence of proton transfer and the formation of a tautomeric form in the excited state may lie in the departure of the proton at position 3 whose hydroxyl is involved in the complex formation. However, this hypothesis is not the only one to be considered as any structural modification due to a complexation reaction could prevent the formation of this tautomeric form. The complexation reaction was also monitored by fluorescence emission spectroscopy, by exciting the solution at the wavelength corresponding to the absorption maximum of the complex (410 nm). The spectral data set (Fig. 3b) also shows the formation of a single fluorescent species. For $R = 0$, a low fluorescence emission is observed at 501 nm; it corresponds to the very small amount of morin in a deprotonated form present in solution at this pH. The complex 1:1 has a maximum

of emission located at 504 nm. The chemometric treatment of the data resulted in a value of log $\beta_{1:1}$ = 4.41 ± 0.2, which is in agreement with the constant calculated at the same pH in absorption spectroscopy.

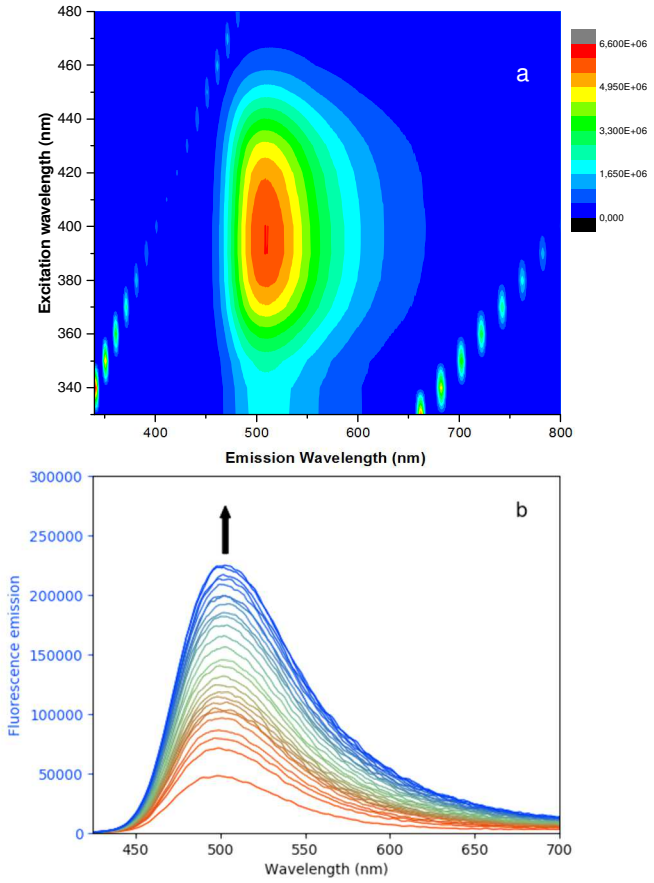

Figure 3: (a) Excitation Emission Matrix of fluorescence of morin-Ca^{II} system at pH = 4.2 for a molar ratio of 2 and (b) Evolution of the fluorescence emission of the complex for molar ratios varying from 0 to 20 at pH = 4.2 (excitation wavelength: 410 nm).

3.2 pH effect on the complexation

As the complexes formed at pH 4.2 and 6.2 are the same, it can be interesting to study the behavior of this complex by varying the pH at a fixed molar ratio. Initially, the spectral evolution of the absorption of the morin-Ca^{II} solution at a molar ratio R = 2 was recorded by varying the pH from 1.84 to 11.29. The resulting spectral data presented in Fig. 4a is complex and requires several decompositions to track the formation of the different species. First of all, at pH 1.84, the complexation is not observed and only the free morin absorbs. With the gradual increase of the pH up to 7.60, the spectrum evolves towards the complex 1:1 highlighted previously (band I at 410 nm) (Fig. 4b). The four isobestic points (238, 259, 289 and 375 nm) present on the spectra confirm the existence of a single equilibrium in solution.

The complexation reaction appears to be total at pH = 7.60 as the spectrum of the free ligand is no longer visible. Then, from pH 7.96 to 9.16, the isobestic points change (250, 270, 361 and 417 nm) and a new bathochromic effect is observed for band I (417 nm) and band II (277 nm). The band I' is now observed at 325 nm. This time, the spectral behavior is typical of a deprotonation, and a new equilibrium is observed between the complex 1:1 and its mono-deprotonated form (Fig. 4c).

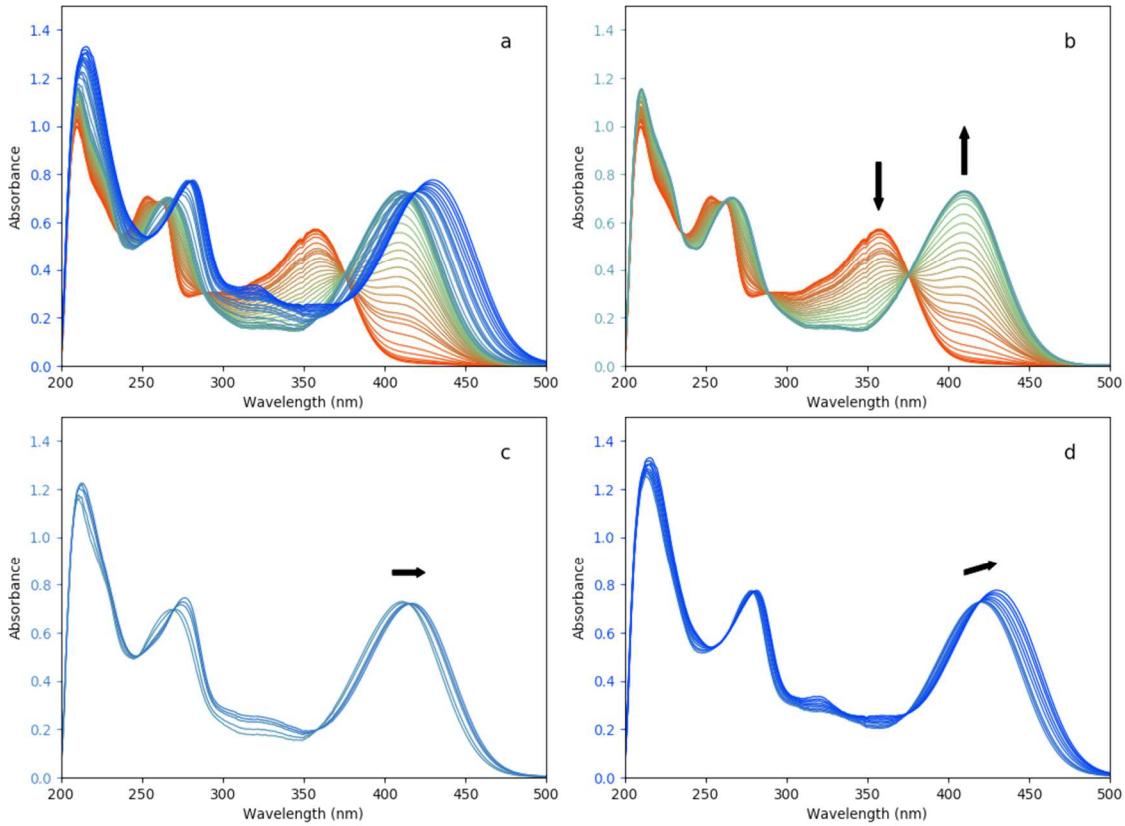

Figure 4: Evolution of the UV-visible spectrum of morin-Ca^{II} system (R = 2) with the pH varying from: (a) 1.84 to 11.29, (b) 1.84 to 7.6, (c) 7.96 to 9.16 and (d) 9.75 to 11.29.

Finally, as from pH 9.75 onwards, the isobestic points change again (259, 281, 378 and 420 nm). New bathochromic effects of 10 nm for band I (427 nm) and 5 nm for band II (282 nm) appear, while the hypsochromic effect continues for the band I' (319 nm). A new equilibrium is highlighted between the mono- and bi-deprotonated forms of the complex (Fig. 4d). If the spectral data clearly shows, on one hand, the formation of the complex and, on the other hand, the successive deprotonation of the latter, it is also possible to obtain, from these data, some thermodynamic quantities such as the formation constant of the complex as well as its first two pK_a values. The change in absorbance plotted at 410 nm with respect to the variation of

the pH from 1.84 to 7.60 has the characteristic shape of a sigmoid curve (Fig. 5a). In the investigated pH range, the absorbance measured at 410 nm can be expressed as:

$$A = \varepsilon_{\mathrm{LH}} l\,[\mathrm{LH}] + \varepsilon_{\mathrm{LCa^+}} l\,[\mathrm{LCa^+}] \qquad (1)$$

To write equation (1), the only equilibrium considered is:

$$\mathrm{LH} + \mathrm{Ca^{2+}} = \mathrm{LCa^+} + \mathrm{H^+} \qquad K \text{ (formation constant)}$$

Notably, the presence of the deprotonated morin is not taken into account that is justified by the results obtained below.

It can be easily shown (using matter conservation and laws of mass action) that the relations:

$$K\,[\mathrm{LH}]^2 + [\mathrm{LH}]\big([\mathrm{H^+}] + c\,K(R-1)\big) - c\,[\mathrm{H^+}] = 0 \qquad (2)$$

and

$$[\mathrm{LCa^+}] = \frac{R\,c\,10^{-\mathrm{p}K_\mathrm{a}}\,[\mathrm{LH}]}{10^{-\mathrm{pH}}c^\circ + 10^{-\mathrm{p}K_\mathrm{a}}\,[\mathrm{LH}]} \qquad (3)$$

hold, with K the complexation constant, c the initial concentration of morin, and c° the standard concentration (1 mol $\mathrm{L^{-1}}$). Thus, the expressions of [LH], from (2), and [$\mathrm{LCa^+}$], from [LH] and (3), lead to an analytical expression of A, that has been computed for each pH value. The parameters, especially K, were optimized using a least-square fitting. A good agreement was obtained depicted on Fig. 5a. Due to the lack of characteristic features, the derivatives were numerically computed both from the fitted model and from the experimental data. Once again, a good agreement was obtained, ensuring that the model reproduce correctly the data.

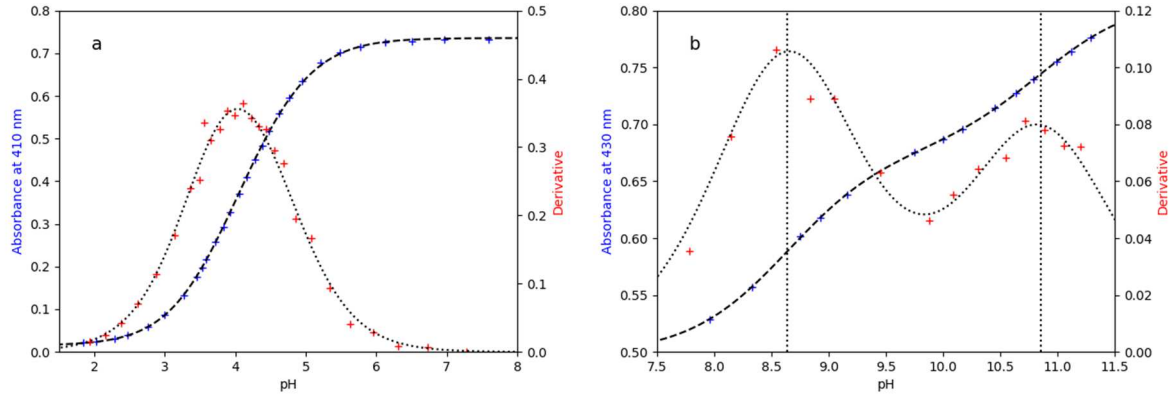

Figure 5: (a) Plot of absorbance at 410 nm with respect to pH (blue +), its derivative function (red +) and fitted model and its derivative and (b) Plot of absorbance at 430 nm with respect to pH (blue +), its derivative function (red +) and fitted model and its derivative. The vertical dotted lines are located at the pH corresponding to extracted pK_a values.

The calculation gives a value of log K of –0.13. As $K = \beta \cdot [H^+]$ and consequently that log β = log K + pH, the values of log β calculated for pH = 4.2 and 6.2 are 4.07 and 6.07 respectively, which are consistent with those obtained from the complexation titration at fixed pH.[47]

In the same way, the variation of the absorbance at 430 nm plotted as a function of the pH between 7.96 and 11.29 shows two inflection points (Fig. 5b), indicating the presence of several equilibria. The obtained curve was treated similarly to the one above.

Nevertheless, the involved equilibria are quite different: two successive deprotonations were hypothesized. In the investigated pH range, the absorbance measured at 430 nm can be expressed as:

$$A = \varepsilon_{LCa^+} l\,[LCa^+] + \varepsilon_{LCa^+(-H^+)} l\,[LCa^+(-H^+)] + \varepsilon_{LCa^+(-2H^+)} l\,[LCa^+(-2H^+)] \qquad (4)$$

To write equation (4), the two equilibria considered are:

$$LCa^+ = LCa^+(-H^+) + H^+ \qquad K_{a1}$$

$$LCa^+(-H^+) = LCa^+(-2H^+) + H^+ \qquad K_{a2}$$

Once again, the presence of the deprotonated morin is not taken into account, which is justified by the results obtained below. Notably, no hypothesis is made either about the number of mono-deprotonated species ($LCa^+(-H^+)$ could stand for several complexes), or about the site of deprotonation. The same holds for the doubly-deprotonated species.

The analytical expressions are more easily writable as in the previous case: It is quite straightforward to derive from matter conservation and laws of mass action:

$$A = c\,l\,\frac{\varepsilon_{LCa^+} 10^{pK_{a1}-pH} + \varepsilon_{LCa^+(-H^+)} + \varepsilon_{LCa^+(-2H^+)} 10^{pH-pK_{a2}}}{10^{pK_{a1}-pH} + 1 + 10^{pH-pK_{a2}}} \qquad (5)$$

with K_{a1} and K_{a2} the acid-base constants defined by the equilibrium above, c the initial concentration in morin, and l the optical path length. Thus, A has been computed for each pH value. The parameters, especially K_{a1} and K_{a2}, were optimized using a least-square fitting. A good agreement was obtained depicted on Fig. 5b. Like in the case of Fig. 5a, the derivatives were numerically computed both from the fitted model and from the experimental data and a good agreement was obtained, ensuring that the model reproduce correctly the data. Remarkably, the pK_a values do not correspond exactly to the inflection points of A and to the maxima of its derivative, due to a small coexistence of both equilibria.

The values of the first two pK_a of the complex 1:1 are 8.6 and 10.9, respectively. However, it is useful to note that these values do not corresponding to the first deprotonation of the morin molecule, which has already undergone deprotonation(s) upon complexation. Thus, these obtained values cannot be easily compared to those of the free ligand.

Afterwards, with identical physicochemical conditions, the same titration followed by fluorescence spectroscopy (Fig. 6) confirms the observations obtained in absorption spectroscopy. The complex emits at 504 nm and then the different deprotonated forms appear with the increase of the pH value. Two new bands of fluorescence appear in the same pH range as the one studied in absorption. As it has been shown by means of the mathematical model that they were mono- and bi-deprotonated forms of the complex, it seems reasonable to assume that these two new emissions correspond to the same forms. Then, the fluorescence emission of the mono-deprotonated form reaches its maximum at 525 nm, whereas the bi-deprotonated form of the complex has an emission centered around 560 nm. Therefore, during successive deprotonations of the complex, the wavelength shifts are more distinguishable in fluorescence than those observed in absorption spectroscopy. The Stokes shifts increase upon deprotonation, and their values are 94, 108 and 133 nm for the complex, the mono- and bi-deprotonated complexed forms respectively.

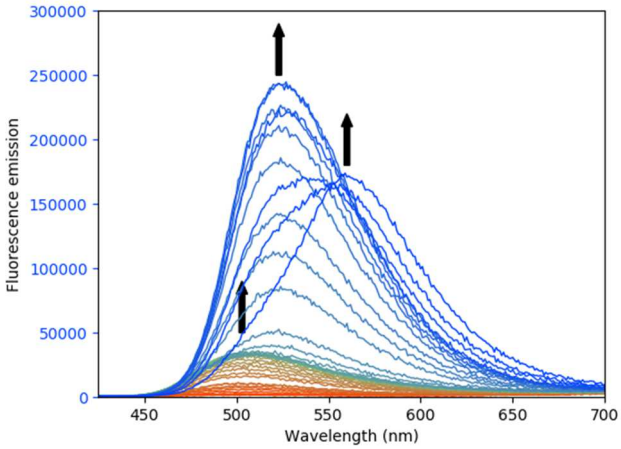

Figure 6: Evolution of the fluorescence spectrum of the morin-Ca^{II} system (R = 2) with pH varying from 1.84 to 11.29 (excitation wavelength: 410 nm)

3.3 Quantum chemistry calculations

Quantum chemistry calculations were performed to determine the structure of the 1:1 complex obtained in acidic medium. To this aim, the possibility of chelation of the metal cation on the four potential sites of the morin was considered. For each site, the competition between Ca^{II} and the proton was taken into account by studying several protonation schemes for the site. For example, for the O2'O3 site, one structure without deprotonation, two structures mono-deprotonated at position 3 or 2', and one doubly deprotonated one were investigated. Moreover, complexation in mono-dentate coordination mode has not been considered because the fixation of Ca^{II} on an ether, carbonyl or hydroxyl function is

chemically unlikely. Finally, the environment of the metal has been studied by varying the coordination number of the latter by adding in its coordination sphere two, three or four solvent molecules. Taking into account these different parameters, there are 30 hypothetical structures whose geometry has been optimized and from which the electronic transitions have been calculated by TD-DFT, in absorption and emission.

The first observation is that the Ca^{II} fixation on the O1O2' site seems impossible. Indeed, whatever the protonation state of the hydroxyl function and the number of solvent molecules in the coordination sphere, no structural optimization has made it possible to obtain a chelated form.

In general, the best agreement between experimental and theoretical spectra is obtained when the metal in the complex is surrounded by four solvent molecules, indicating that calcium adopts an octahedral environment in this complex. The comparison of the results obtained with a different number of solvent molecules will be discussed later. The overlay of the experimental spectrum of the 1:1 complex obtained in acidic conditions with the positions of the electronic transitions calculated for the remaining eight structural hypotheses that exhibit hexa-coordinated calcium is presented in Fig. 7.

The hypothetical structures will be noted as compOxOy with x and y having the values 2', 3, 4 or 5 corresponding to the positions on the ligand. For example, compO2'O3 corresponds to a chelate which involves the two hydroxyl functions O2'H and O3H. The symbol -H denotes a deprotonation of a hydroxyl group involved in the fixation of the calcium atom. Thus, comp O2'O3-H implies the same site as in the previous example but the site is mono-deprotonated in position 3. The observation of the theoretical spectra (represented by vertical lines) in Fig. 7 shows a large number of electronic transitions calculated in the short wavelength range. It is therefore difficult to obtain relevant information on band II of the UV-vis spectrum since, in all cases, the calculated transitions allow a good depiction of this band. Due to that, we focused mainly on band I (410 nm) but also on the weak band I' (~330 nm). Even though for comparison purposes the spectra of all hypothetical forms are shown in Fig. 7, it is possible to rule out the three fully protonated forms: compO4O5, compO3O4 and compO2'O3 (Fig. 7a, 7c and 7e, respectively) from the computed data and because of their little chemical meaning. Indeed, a decrease in the pH of the solution is observed at each addition of calcium salt until the end of the assay, which indicates a deprotonation of the cation binding site. Moreover, we observe that the transitions computed in the long wavelength range for these complexes are blue shifted compared to the experimental spectrum.

The HOMO→LUMO transition (98%) of compO4O5-H (Fig. 7b) is well calculated (412 nm) with respect to the experimental wavelength of the band I while the band I' is described by a transition involving the HOMO−1→LUMO (97%) whose oscillator strength is too high (f = 0.38). It means that the oscillator strength of the band I' is calculated 1.5 times higher than that of the band I while its measured absorbance is about 50 times lower. Hence, the compO4O5-H spectrum does not satisfactorily reproduce the spectrum of the 1:1 complex and

the involvement of the O4O5 site in the Ca^{II} binding can be ruled out. This confirms the observation already made in the experimental part (involvement of position 3).

The calculated spectrum of compO3-HO4 (Fig. 7d) reproduces the experimental absorption spectrum particularly well. Band I is described by the HOMO→LUMO transition (98%) calculated at 415 nm with an oscillator strength of 0.52, while band I' is represented by two low probability transitions (f = 0.03 and 0.05) calculated at 338 (HOMO−1→LUMO, 97%) and 315 nm (HOMO−2→LUMO, 93%) respectively. The calculated fluorescence emission of this complex (526 nm) is also in agreement with the experimental one (504 nm). Thus, Ca^{II} chelation on the deprotonated O3O4 site is a highly probable hypothesis. In the same way, the implication of the O2'O3 fully deprotonated site in the formation of the complex is possible. The HOMO→LUMO transition (97%) of compO2'-HO3-H (Fig. 7f) is calculated at 422 nm, that is 0.08 eV lower in energy than the observed transition. Band I' is depicted by two weak transitions located at 357 and 311 nm (ΔE = 0.28 and 0.23 eV from the experimental band, respectively). For this complex, a fair agreement is observed for the emission wavelength (522 nm versus 504 nm). The same chelating site with a single deprotonation in the 2' position has been considered and the results of the calculation are shown in Fig. 7g. Band I is rather well represented by the HOMO→LUMO transition (99%) calculated at 416 nm (f = 0.30) but a second transition computed at 350 nm with a large oscillator strength (0.20) has led to doubt the presence of compO3O2'-H in solution. This species can be definitively ruled out because its fluorescence emission is calculated at 569 nm far from the experimental value observed at 504 nm. The last hypothesis is compO3-HO2' whose theoretical spectrum is shown in Fig. 7h. The lowest energy transition (HOMO→LUMO 98%) calculated at 401 nm (f = 0.40) reproduces fairly the position and the absorbance of band I, while a single transition computed at 314 nm (f = 0.05) is likely to represent band I'. The fluorescence wavelength of this hypothetical structure has been estimated at 499 nm, in good agreement with the experimental value. From a spectral point of view, this structure cannot be excluded. However, from an energetical point of view, compO3-HO2' can be compared to compO3O4 because they have the same number of atoms and both involve a single deprotonation. Thermodynamic calculations show that compO3-HO2' has a Gibbs free energy greater than compO3O4 of ($\Delta_r G$ = 14.3 kcal mol^{-1}). This kind of calculation being challenging, the same calculations were carried out with two other different hybrid density functionals: the M06-2X and ωB97X-D considered as robust functionals for the description of energy.[48-49] The values found for the energy difference have the same order of magnitude; they are of 12.1 and 10.7 kcal mol^{-1}, respectively for these two functionals. This significant energy difference leads to eliminate the structure exhibiting calcium chelation on the di-hydroxyl function with a deprotonation in position 3. At this stage, the comparison of the calculated electronic transitions with the absorption and emission spectra leads to two structural hypotheses: compO3-HO4 and compO2'-HO3-H (Fig. 8a).

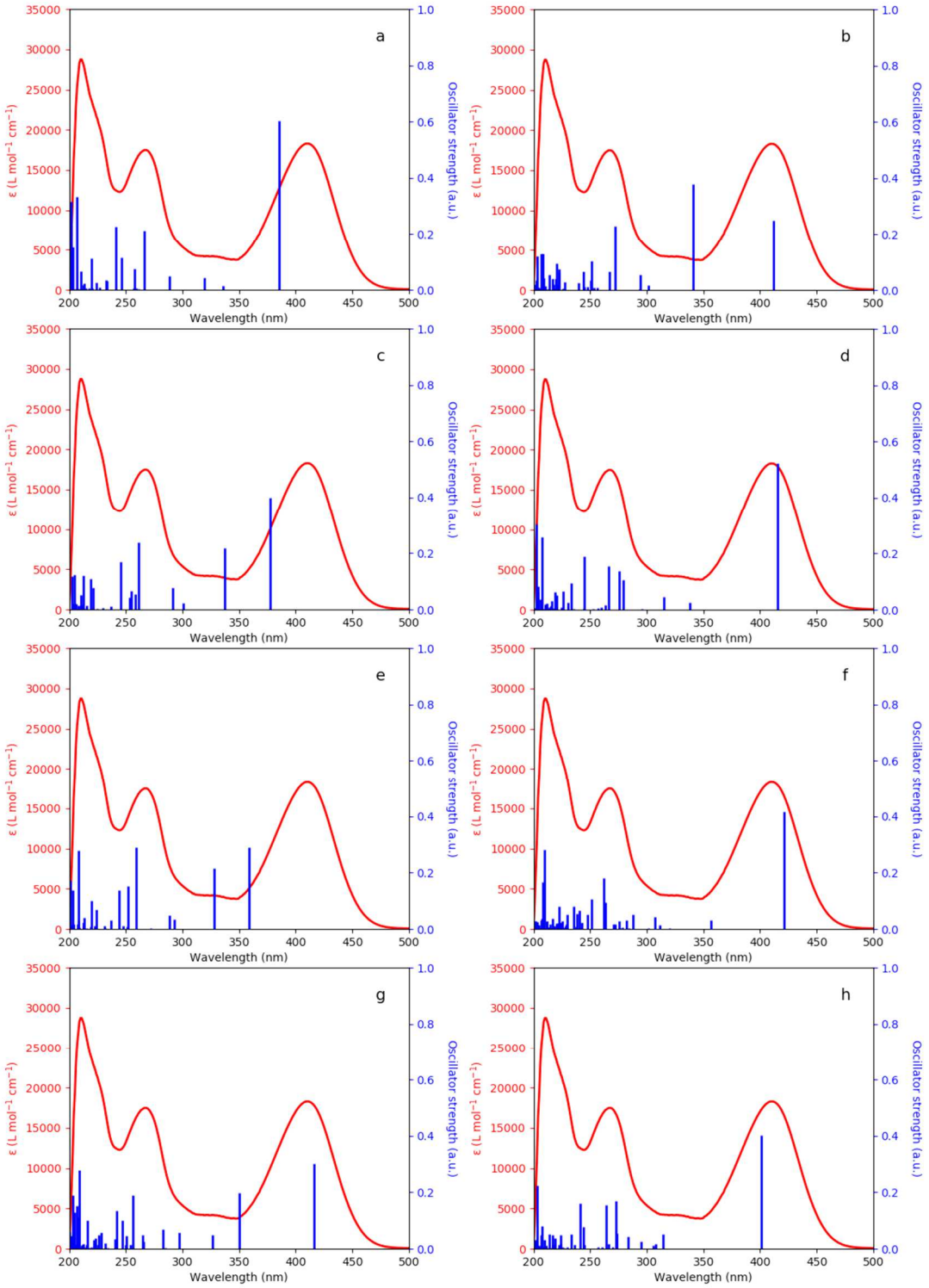

Figure 7: Experimental spectrum of the complex 1:1 (red) and theoretical electronic transitions (blue lines) calculated for different hypothetical structures: (a) compO4O5, (b) compO4O5-H, (c) compO3O4, (d) compO3-HO4, (e) compO2'O3, (f) compO2'-HO3-H, (g) compO3O2'-H and (h) compO3-HO2'

The influence of the number of solvent molecules within the metal coordination sphere is illustrated by means of the calculated electronic transitions in Fig. S1 (supporting information). In some cases, the influence is minor and the wavelengths of the electronic transitions are calculated within a few nanometers, this is the case for compO3-HO4 (Fig. S1a). In contrast, the binding of calcium with the di-hydroxyl function in the position 2',3 is likely to cause steric hindrance depending on the number of solvent molecules in the coordination sphere of the metal cation and leads to more significant differences in the calculated wavelengths as shown in Fig. S1b for compO2'-HO3.

Although successive deprotonations have been considered for all hypothetical structures, we will focus, in the remaining part of the paper, on compO3-HO4 and compO2'-HO3-H structures, with the departure of the most labile protons of the complex. In a first step, for both complexes, the deprotonations of OH4', OH7 groups or one molecule of water in the coordination sphere of Ca have been considered (an increase in pH is likely to deprotonate a water molecule leading to a ligand in the form of HO^-). For compO3-HO4, the deprotonation of OH2' function has also been envisaged. The structures of the ground state and the first excited state of the mono-deprotonated complexes have been optimized and the electronic transitions have been calculated in absorption and emission.

The computed absorption wavelengths corresponding to the lowest energy transition (HOMO→LUMO) as well as those calculated for fluorescence emission are reported in Fig. 8b for all the first deprotonation assumptions of the 1:1 complex. These calculated values should be compared with those observed experimentally, i.e. 417 and 525 nm, respectively. It can be noted that, for the two complexed forms, the deprotonation of a solvent molecule in the coordination sphere of calcium leads to wavelengths in very good agreement with the experimental values both in terms of absorption and in emission. This agreement is very good for compO3-HO4 where the energy differences between the calculated and experimental values for the electronic transitions are around 0.02 eV. Besides, the whole spectrum of the mono-deprotonated 1:1 complex is well reproduced by the electronic transitions calculated with a deprotonation of a water molecule in the coordination sphere of the metal cation (Fig. S2.c). By contrast, the experimental spectrum is less correctly reproduced by the calculated spectrum corresponding to the deprotonation of a water molecule of compO2'-HO3-H (Fig. S2.a). The deprotonation of the OH7 function of compO2'-HO3-H leads to the calculation of absorption and emission wavelengths which correspond very well to the experimental values. In addition, the calculated transitions perfectly reproduce the absorption spectrum of the mono-deprotonated complex (Fig. S2.b). The deprotonation of the other hydroxyl functions (the position 4' for compO2'-HO3-H and the positions 2', 4 'or 7 for compO3-HO4) lead either to calculated HOMO→LUMO wavelengths too far from the values observed experimentally (Fig. 8b) or to important discrepancies between the theoretical and experimental data in the higher energy range. For these reasons, these hypotheses of first deprotonation were not retained. Thus, only three mono-deprotonated complexed forms were retained, two corresponding to the presence of a hydroxide group in the Ca coordination sphere, which will be noted as compO2'-HO3-H_OH^- and compO3-HO4_OH^- as well as the

deprotonation of the hydroxyl in position 7 of compO2'-HO3-H which will be noted as compO2'-HO3-H_O7-H.

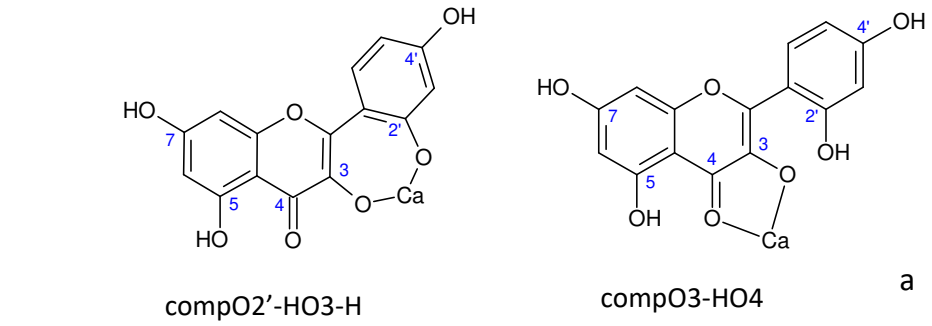

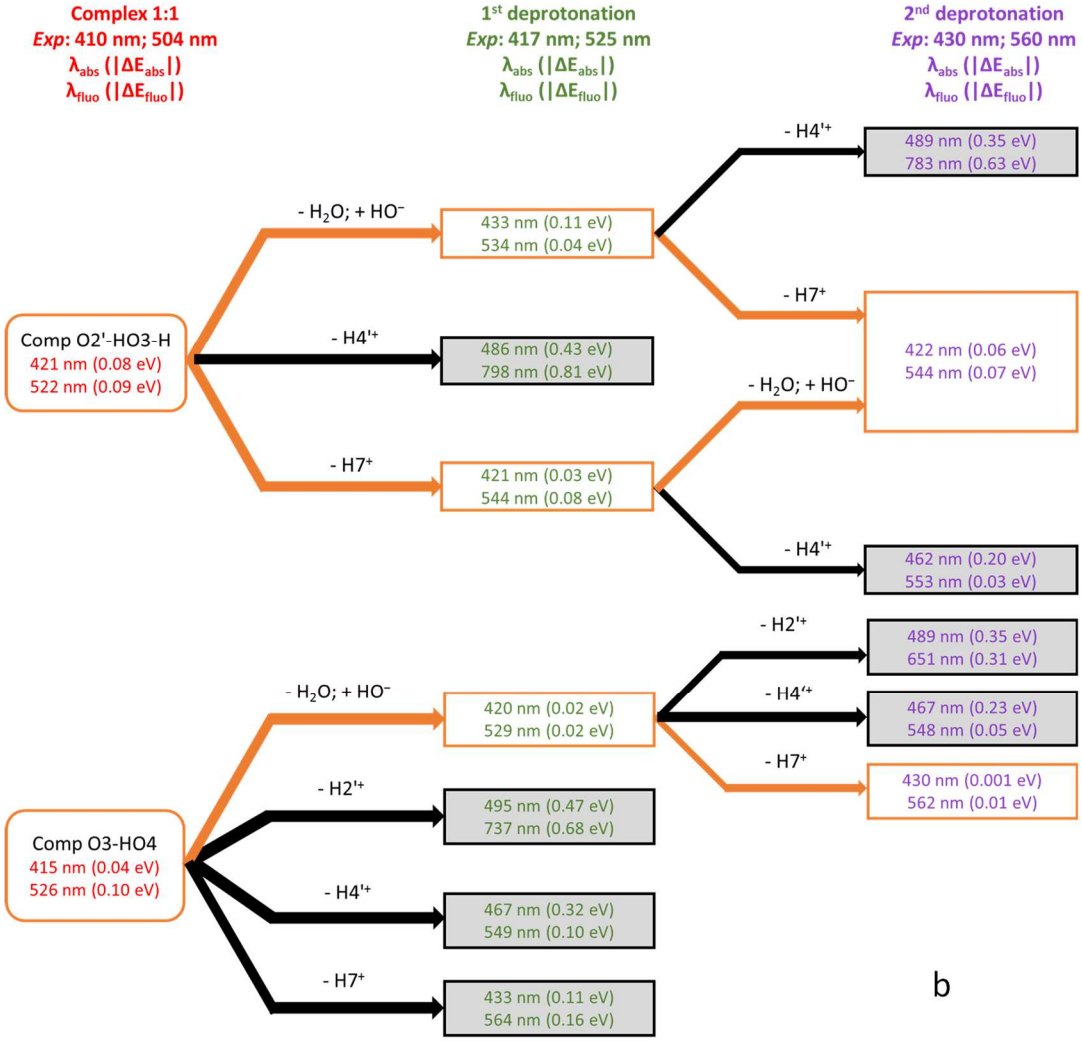

Figure 8: (a) Structures of compO3-HO4 and compO2'-HO3-H (solvent molecules have been omitted). (b) Experimental absorption and emission wavelengths of the complex 1:1 and its two deprotonated forms and calculated absorption (HOMO→LUMO transition) and fluorescence wavelengths for the different hypothesis of complex deprotonation. The values in brackets are the difference between the calculated and experimental energy transitions (in absolute values).

From these three mono-deprotonated forms, a second deprotonation has been investigated involving the same functions as those previously considered for the first one. The calculated absorption (HOMO→LUMO) and fluorescence wavelengths reported in the right part of Fig. 8b for the different doubly deprotonated hypothesis should be compared to those observed experimentally: 430 and 560 nm respectively. The deprotonation of position 7 of compO2'-HO3-H_OH^- and the deprotonation of a water molecule of compO2'-HO3-H_O7-H lead to the same complex named compO2'-HO3-H_O7-H_OH^- (Fig. S2.d), which has theoretical wavelengths in good adequacy with the expected values. In the same way, the deprotonation in position 7 of compO3-HO4_OH^- gives satisfactory results with respect to the experimental values (Fig. S2.e). TD-DFT computations on the optimized structure, where the second deprotonation involves the other functions, lead to results too far from the experimental values and can be discarded. Quantitatively, the wavelengths calculated for compO3-HO4 and its two successive deprotonations are closer to the experimental values than those obtained from derivatives compO2'-HO3-H. However, it seems difficult to exclude them only on the basis of the spectral aspect, which is why the energy features have also been studied.

In order to compare the free enthalpies of the complexes, it was necessary to take into account the solvation free energy of the proton (−257 kcal mol^{-1}) insofar as all complexes are not at the same level of deprotonation.[50] CompO2'-HO3-H has a Gibbs free energy 32.2 kcal mol^{-1} higher than compO3-HO4. Likewise, compO2'-HO3-H_O7-H and compO2'-HO3-H_OH^- have free energy values of 38.2 and 40.9 kcal mol^{-1} higher than compO3-HO4_OH^- respectively. Finally, compO2'-HO3-H_OH^-_O7-H lies 46.6 kcal mol^{-1} higher than compO3-HO4_OH^-_O7-H. These values should be carefully compared because of a quite important effect of entropical factors and of the uncertainty on the value of the solvation free energy of the proton. Nevertheless, in the case of interest, the computed differences are large enough to suggest an interpretation. Thus, the fact that the whole deprotonation path of compO3-HO4 lies below the one of compO2'-HO3-H is consistent with a Ca^{II} chelation that would take place with the deprotonated 3-hydroxy-keto site. Then, a progressive increase in pH induces successively a first deprotonation of a solvent molecule located in the coordination sphere of the metal and a second deprotonation of the hydroxyl function at position 7, as illustrated in Fig. 9.

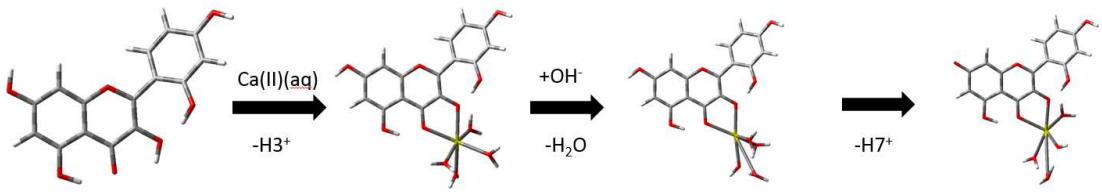

Figure Reaction scheme illustrating the regio-selectivity of Ca^{II} binding by morin and the two successive deprotonations of the formed complex.

The main structural modifications of the ligand which occur with the complexation or the successive deprotonations of the obtained complex are listed in Table 1. As expected, the different C3O3 and C4O4 bond lengths in morin tend to get much closer with the chelate formation even though the C3O3 bond remains longer than C4O4 in the calcium-containing ring. The inter-ring bond increases in the complexes with respect to the free ligand, which would indicate a decrease in the electronic delocalization over the entire molecule. However, the inter-ring dihedral angle decreases for the complexed forms, this could be due to the increase of the strength of the intra-molecular hydrogen bond H2'O3. The deprotonation of a solvent molecule in the coordination sphere of calcium hardly changes the structure of the ligand. This observation depicts the strong ionic nature of the metal-ligand bonds. Finally, the deprotonation of the hydroxyl function in position 7 has a much greater impact on the geometry of the ligand even at the metal binding site.

Table 1: Main geometrical parameters for morin and its complexes with Ca^{II}, at different pH values. The bond lengths are given in Å and the inter-ring dihedral angle is in °.

	morin	compO3-HO4	compO3-HO4_OH^-	compO3-HO4_OH^-_O7-H
C2C1'	1.459	1.465	1.465	1.469
C3O3	1.359	1.327	1.323	1.335
C4O4	1.254	1.279	1.279	1.289
O3Ca		2.356	2.355	2.405
O4Ca		2.389	2.398	2.371
H2'O3	1.701	1.508	1.490	1.505
C3C2C1'C2'	−35.9	−29.7	−29.1	−31.1

4. Conclusions

The morin molecule forms a stable mono-cationic complex with Ca^{II} in methanol solution. The combination of electronic spectroscopies and quantum chemical calculations has shown that, among the four chelating sites in competition for the fixation of this alkaline earth metal cation, the 3-hydroxy-keto group is the preferential site. The selectivity found in binding Ca^{II}, even at low pH is an important result considering the biological importance of such ions. The chelation occurs with a full deprotonation of the 3-hydroxyl function. As a consequence, an increase in pH raises the affinity of morin for Ca^{II}. From a pH value of 7.60, the deprotonation of the complex starts and the quantum chemistry calculations have shown that it is not a deprotonation of the ligand but that of a solvent molecule present in the coordination sphere of the complex. A pH of 9.75 must be reached to remove a proton from the hydroxyl function in position 7 of complexed morin; the pK_a of this function is estimated to be around 10.9.

It is interesting to note that the same work was done on the complexation of Ca^{II} with quercetin (3, 3', 4', 5, 7-pentahydroxyflavone) and luteolin (3', 4', 5, 7-tetrahydroxyflavone) (unpublished results). For the case of quercetin, a very large amount of calcium is required to observe a complex (molar ratio in the order to 500), whereas with luteolin, no complex presence could be demonstrated even with high concentrations of calcium salt. These results show that the hydroxyl function at the position 3 is essential for the formation of a complex with Ca^{II} insofar as it is not observed with luteolin. However, they also show that the 2' hydroxyl group plays a key role in the affinity of morin for calcium. As we have described in a previous paper, the intramolecular hydrogen bond network created from hydroxyl functions at the 2' and 3 positions plays a significant role in the reactivity of morin.[8]

Finally, it should be noted that if other spectroscopic techniques such as ^{1}H NMR and infrared coupled to quantum chemistry calculations can be useful to determine the preferential complexation site of flavonoids.[51] These techniques, however, remain limited especially because of the high concentrations of necessary metal salts which prohibit the study as a function of the pH. Indeed, a pH increase will produce a precipitation of metal hydroxide which would distort the measurements.

Acknowledgments

The CaPPA project (Chemical and Physical Properties of the Atmosphere) is funded by the French National Research Agency (ANR) through the PIA (Programme d'Investissement d'Avenir) under the contract “ANR-11-LABX-0005-01” and by the Regional Council “Hauts-de-France” and the European Regional Development Fund (ERDF). This work is also a contribution to the CPER research project CLIMIBIO.

This work was granted access to the HPC resources of CINES (Centre Informatique National de l’Enseignement Superieur) and IDRIS (Institut du Developpement et des Ressources en Informatique Scientifique) under the allocations A0030806933 and A0050806933 made by GENCI (Grand Equipement National de Calcul Intensif). We also thank the CRI (Centre de Ressources Informatiques) of the University of Lille for providing computation time for part of the calculations.

References

1. Panche, A. N.; Diwan, A. D.; Chandra, S. R., Flavonoids: An Overview. *J. Nutr. Sci.* **2016**, *5*, e47.
2. Jovanovic, S. V.; Steenken, S.; Tosic, M.; Marjanovic, B.; Simic, M. G., Flavonoids as Antioxidants. *J. Am. Chem. Soc.* **1994**, *116*, 4846-4851.
3. de Souza, R. F. V.; De Giovani, W. F., Antioxidant Properties of Complexes of Flavonoids with Metal Ions. *Redox Rep.* **2004**, *9*, 97-104.
4. Karak, P., Biological Activities of Flavonoids: An Overview. *Int. J. Pharm. Sci. Res.* **2019**, *10*, 1567-1574.
5. Gorniak, I.; Bartoszewski, R.; Kroliczewski, J., Comprehensive Review of Antimicrobial Activities of Plant Flavonoids. *Phytochem. Rev.* **2019**, *18*, 241-272.
6. Kumar, H.; Agrawal, R.; Kumar, V., Barleria Cristata: Perspective Towards Phytopharmacological Aspects. *J. Pharm. Pharmacol.* **2018**, *70*, 475-487.
7. Solanki, I.; Parihar, P.; Mansuri, M. L.; Parihar, M. S., Flavonoid-Based Therapies in the Early Management of Neurodegenerative Diseases. *Adv. Nutr.* **2015**, *6*, 64-72.
8. Moncomble, A.; Jani Thaviligadu, D.; Raoumbé Djendja, A.; Cornard, J.-P., The Crucial Role of the Inter-Ring Hydrogen Bond to Explain the Properties of Morin. *New J. Chem.* **2018**, *42*, 7691-7702.
9. Dominguez-Renedo, O.; Navarro-Cunado, A. M.; Ventas-Romay, E.; Alonso-Lomillo, M. A., Determination of Aluminium Using Different Techniques Based on the Al(Iii)-Morin Complex. *Talanta* **2019**, *196*, 131-136.
10. Kokulnathan, T.; Sakthinathan, S.; Chen, S. M.; Karthik, R.; Chiu, T. W., Hexammine Cobalt(Iii) Coordination Complex Grafted Reduced Graphene Oxide Composite for Sensitive and Selective Electrochemical Determination of Morin in Fruit Samples. *Inorg. Chem. Front.* **2018**, *5*, 1145-1155.
11. Sentkowska, A.; Kilian, K.; Kopec, M.; Pyrzynska, K.; Cheda, L., Ga(Iii) Complex with Morin for Kidney Cancer Cell Labelling. *Appl. Organomet. Chem.* **2017**, *31*.
12. Woznicka, E.; Zapala, L.; Pieniazek, E.; Kosinska, M.; Ciszkowicz, E.; Lecka-Szlachta, K.; Pusz, J.; Maciolek, U.; Dronka, J., Synthesis, Characterization and Antibacterial Studies of Tm(Iii), Yb(Iii) and Lu(Iii) Complexes of Morin. *J. Coord. Chem.* **2017**, *70*, 1451-1463.
13. Pieniazek, E.; Kalembkiewicz, J.; Dranka, M.; Woznicka, E., Syntheses, Crystal Structures and Antioxidant Study of Zn(Ii) Complexes with Morin-5 '-Sulfonic Acid (Msa). *J. Inorg. Biochem.* **2014**, *141*, 180-187.
14. Liu, E.; Zhang, H. X., Interaction of the La(Iii)-Morin Complex with Human Serum Albumin. *J. Sol. Chem.* **2014**, *43*, 1402-1413.
15. Panhwar, Q. K.; Memon, S., Synthesis and Properties of Zirconium(Iv) and Molybdate(Ii) Morin Complexes. *J. Coord. Chem.* **2012**, *65*, 1130-1143.
16. Jabeen, E.; Janjua, N. K.; Ahmed, S.; Murtaza, I.; Ali, T.; Masood, N.; Rizvi, A. S.; Murtaza, G., Dft Predictions, Synthesis, Stoichiometric Structures and Anti-Diabetic Activity of Cu (Ii) and Fe (Iii) Complexes of Quercetin, Morin, and Primuletin. *J. Mol. Struct.* **2017**, *1150*, 459-468.
17. Roy, A. S.; Samanta, S. K.; Ghosh, P.; Tripathy, D. R.; Ghosh, S. K.; Dasgupta, S., Cell Cytotoxicity and Serum Albumin Binding Capacity of the Morin-Cu(Ii) Complex and Its Effect on Deoxyribonucleic Acid. *Mol. Biosyst.* **2016**, *12*, 2818-2833.
18. Sendrayaperumal, V.; Pillai, S. I.; Subramanian, S., Design, Synthesis and Characterization of Zinc-Morin, a Metal Flavonol Complex and Evaluation of Its Antidiabetic Potential in Hfd-Stz Induced Type 2 Diabetes in Rats. *Chem. Biol. Interact.* **2014**, *219*, 9-17.
19. Naso, L. G.; Lezama, L.; Rojo, T.; Etcheverry, S. B.; Valcarcel, M.; Roura, M.; Salado, C.; Ferrer, E. G.; Williams, P. A. M., Biological Evaluation of Morin and Its New Oxovanadium(Iv) Complex as Antio-Xidant and Specific Anti-Cancer Agents. *Chem. Biol. Interact.* **2013**, *206*, 289-301.
20. Broadley, M. R.; White, P. J., Calcium in Plants. *Ann. Bot.* **2003**, *92*, 487-511.

21. George, T. S.; White, P. J.; Neugebauer, K.; Broadley, M. R.; El-Serehy, H. A., Linear Relationships between Shoot Magnesium and Calcium Concentrations among Angiosperm Species Are Associated with Cell Wall Chemistry. *Ann. Bot.* **2018**, *122*, 221-226.
22. Calì, T.; Ottolini, D.; Brini, M., Mitochondrial Ca2+ and Neurodegeneration. *Cell Calcium* **2012**, *52*, 73-85.
23. Calì, T.; Ottolini, D.; Brini, M., Chapter 27 Mitochondrial Calcium Homeostasis and Implications for Human Health. In *Calcium: Chemistry, Analysis, Function and Effects*, The Royal Society of Chemistry: 2016; pp 448-467.
24. Brini, M.; Calì, T.; Ottolini, D.; E., C., Intracellular Calcium Homeostasis and Signaling. In *Metallomics and the Cell. Metal Ions in Life Sciences*, (eds), I. B. L., Ed. Springer: Dordrecht, 2013; Vol. 12.
25. Carafoli, E., Calcium Signaling: A Tale for All Seasons. *Proc. Natl. Acad. Sci. USA* **2002**, *99*, 1115-1122.
26. Le Person, A.; Moncomble, A.; Cornard, J. P., The Complexation of Al-Iii, Pb-Ii, and Cu-Ii Metal Ions by Esculetin: A Spectroscopic and Theoretical Approach. *J. Phys. Chem. A* **2014**, *118*, 2646-2655.
27. Moncomble, A.; Falantin, C.; Cornard, J. P., Electronic Spectroscopies Combined with Quantum Chemistry Calculations: Study of the Interactions of 3-Hydroxyflavone with Copper Ions. *J. Phys. Chem. B* **2018**, *122*, 8943-8951.
28. *Reactlab Equilibria*, version 1.00; Jplus Consulting PTY Ltd: Australia.
29. Gampp, H.; Maeder, M.; Meyer, C. J.; Zuberbühler, A. D., Calculation of Equilibrium Constants from Multiwavelength Spectroscopic Data—Iv: Model-Free Least-Squares Refinement by Use of Evolving Factor Analysis. *Talanta* **1986**, *33*, 943-951.
30. Maeder, M.; Zuberbuehler, A. D., Nonlinear Least-Squares Fitting of Multivariate Absorption Data. *Anal. Chem.* **1990**, *62*, 2220-2224.
31. Frisch, M. J. T., G. W.; Schlegel, H. B.; Scuseria, G. E.; Robb, M. A.; Cheeseman, J. R.; Scalmani, G.; Barone, V.; Mennucci, B.; Petersson, G. A.; Nakatsuji, H.; Caricato, M.; Li, X.; Hratchian, H. P.; Izmaylov, A. F.; Bloino, J.; Zheng, G.; Sonnenberg, J. L.; Hada, M.; Ehara, M.; Toyota, K.; Fukuda, R.; Hasegawa, J.; Ishida, M.; Nakajima, T.; Honda, Y.; Kitao, O.; Nakai, H.; Vreven, T.; Montgomery, J. A., Jr.; Peralta, J. E.; Ogliaro, F.; Bearpark, M.; Heyd, J. J.; Brothers, E.; Kudin, K. N.; Staroverov, V. N.; Kobayashi, R.; Normand, J.; Raghavachari, K.; Rendell, A.; Burant, J. C.; Iyengar, S. S.; Tomasi, J.; Cossi, M.; Rega, N.; Millam, J. M.; Klene, M.; Knox, J. E.; Cross, J. B.; Bakken, V.; Adamo, C.; Jaramillo, J.; Gomperts, R.; Stratmann, R. E.; Yazyev, O.; Austin, A. J.; Cammi, R.; Pomelli, C.; Ochterski, J. W.; Martin, R. L.; Morokuma, K.; Zakrzewski, V. G.; Voth, G. A.; Salvador, P.; Dannenberg, J. J.; Dapprich, S.; Daniels, A. D.; Farkas, Ö.; Foresman, J. B.; Ortiz, J. V.; Cioslowski, J.; Fox, D.J. *Gaussian 09, Revision E.01*, 2009.
32. Kohn, W.; Becke, A. D.; Parr, R. G., Density Functional Theory of Electronic Structure. *J. Phys. Chem.* **1996**, *100*, 12974-12980.
33. Becke, A. D., Density-Functional Exchange-Energy Approximation with Correct Asymptotic Behavior. *Phys. Rev. A* **1988**, *38*, 3098-3100.
34. Lee, C. T.; Yang, W. T.; Parr, R. G., Development of the Colle-Salvetti Correlation-Energy Formula into a Functional of the Electron-Density. *Phys. Rev. B* **1988**, *37*, 785-789.
35. Krishnan, R.; Binkley, J. S.; Seeger, R.; Pople, J. A., Self-Consistent Molecular Orbital Methods. Xx. A Basis Set for Correlated Wave Functions. *J. Chem. Phys.* **1980**, *72*, 650-654.
36. McLean, A. D.; Chandler, G. S., Contracted Gaussian Basis Sets for Molecular Calculations. I. Second Row Atoms, Z=11–18. *J. Chem. Phys.* **1980**, *72*, 5639-5648.
37. Hariharan, P. C.; Pople, J. A., The Influence of Polarization Functions on Molecular Orbital Hydrogenation Energies. *Theor. Chim. Acta* **1973**, *28*, 213-222.
38. Cossi, M.; Scalmani, G.; Rega, N.; Barone, V., New Developments in the Polarizable Continuum Model for Quantum Mechanical and Classical Calculations on Molecules in Solution. *J. Chem. Phys.* **2002**, *117*, 43-54.

39. Tomasi, J.; Mennucci, B.; Cammi, R., Quantum Mechanical Continuum Solvation Models. *Chem. Rev.* **2005**, *105*, 2999-3094.
40. Boumendil, S.; Cornard, J.-P.; Sekkal-Rahal, M.; Moncomble, A., Solvent Effects to Compute Uv–Vis Spectra for Ionic Metal Complexes. *Chem.l Phys. Lett.* **2015**, *636*, 39-45.
41. Woźnicka, E.; Kopacz, M.; Umbreit, M.; Kłos, J., New Complexes of La(Iii), Ce(Iii), Pr(Iii), Nd(Iii), Sm(Iii), Eu(Iii) and Gd(Iii) Ions with Morin. *J. Inorg. Biochem.* **2007**, *101*, 774-782.
42. Ameer-Beg, S.; Ormson, S. M.; Brown, R. G.; Matousek, P.; Towrie, M.; Nibbering, E. T. J.; Foggi, P.; Neuwahl, F. V. R., Ultrafast Measurements of Excited State Intramolecular Proton Transfer (Esipt) in Room Temperature Solutions of 3-Hydroxyflavone and Derivatives. *J. Phys. Chem. A* **2001**, *105*, 3709-3718.
43. Brucker, G. A.; Swinney, T. C.; Kelley, D. F., Proton-Transfer and Solvent Polarization Dynamics in 3-Hydroxyflavone. *J. Phys. Chem.* **1991**, *95*, 3190-3195.
44. Mezzetti, A.; Protti, S.; Lapouge, C.; Cornard, J. P., Protic Equilibria as the Key Factor of Quercetin Emission in Solution. Relevance to Biochemical and Analytical Studies. *Phys. Chem. Chem. Phys.* **2011**, *13*, 6858-6864.
45. Yang, D. P.; Yang, G.; Zhao, J. F.; Zheng, R.; Wang, Y. S.; Lv, J., A Theoretical Assignment on Excited-State Intramolecular Proton Transfer Mechanism for Quercetin. *J. Phys. Org. Chem.* **2017**, *30*.
46. Simkovitch, R.; Huppert, D., Excited-State Intramolecular Proton Transfer of the Natural Product Quercetin. *J. Phys. Chem. B* **2015**, *119*, 10244-10251.
47. Herrero-Martinez, J. M.; Repolles, C.; Bosch, E.; Roses, M.; Rafols, C., Potentiometric Determination of Aqueous Dissociation Constants of Flavonols Sparingly Soluble in Water. *Talanta* **2008**, *74*, 1008-1013.
48. Zhao, Y.; Truhlar, D. G., The M06 Suite of Density Functionals for Main Group Thermochemistry, Thermochemical Kinetics, Noncovalent Interactions, Excited States, and Transition Elements: Two New Functionals and Systematic Testing of Four M06-Class Functionals and 12 Other Functionals. *Theor. Chem. Acc.* **2008**, *120*, 215-241.
49. Chai, J.-D.; Head-Gordon, M., Long-Range Corrected Hybrid Density Functionals with Damped Atom–Atom Dispersion Corrections. *Phys. Chem. Chem. Phys.* **2008**, *10*, 6615-6620.
50. Fifen, J. J.; Nsangou, M.; Dhaouadi, Z.; Motapon, O.; Jaidane, N. E., Solvation Energies of the Proton in Methanol. *J. Chem. Theory Comput.* **2013**, *9*, 1173-1181.
51. De Souza, L. A.; Soeiro, M. M.; De Almeida, W. B., A Dft Study of Molecular Structure and 1h Nmr, Ir, and Uv-Vis Spectrum of Zn(Ii)-Kaempferol Complexes: A Metal-Flavonoid Complex Showing Enhanced Anticancer Activity. *Int. J. Quantum Chem.* **2018**, *118*, e25773.